AIAA-2003-3632

# Detached Eddy Simulation Of Turbine Blade Cooling

Sagar Kapadia and Subrata Roy
Computational Plasma Dynamics Laboratory
Kettering University, Flint, Michigan

James Heidmann
NASA Glenn Research Center
Cleveland, Ohio

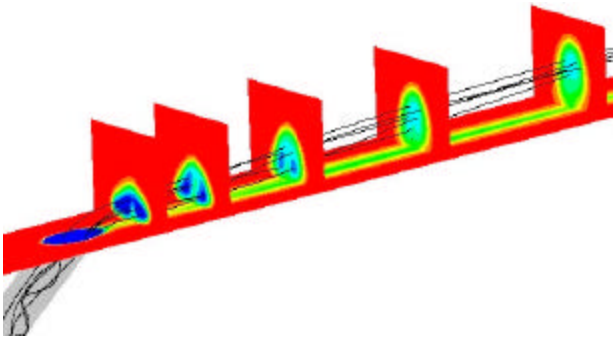

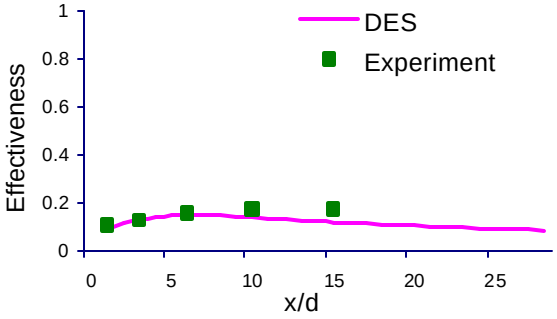


**36th Thermophysics Conference**
23-26 June 2003
Orlando, Florida

# Detached Eddy Simulation of Turbine Blade Cooling

**Sagar Kapadia[1] and Subrata Roy[2]**
*Computational Plasma Dynamics Laboratory*
*Department of Mechanical Engineering*
*Kettering University, Flint, Michigan 48504, USA*

**James Heidmann[3]**
*NASA Glenn Research Center*
*Cleveland, Ohio USA*

Implementation of direct numerical simulation or large eddy simulation for turbomachinery applications is very expensive with present day computational power. Present work explores the possibility of detached eddy simulation (DES) for the film cooled flat plate. A geometry of single row of 35 degree round holes on a flat plate is used for the blowing ratio of 1.0 and density ratio of 0.5. Use of symmetry boundary condition is avoided to capture three-dimensional, unsteady, turbulent nature of the flow. Present simulation uses unstructured grid and parallel algorithm to perform DES. Implicit time-stepping is used for the CFL number upto one million. Presence of asymmetry in the DES solution is documented by plotting the temperature and velocity profiles at various streamwise locations. Numerical calculation of effectiveness is validated with reported experimental results.

## INTRODUCTION

Understanding the interaction between cold fluid jets and hot cross-stream is very important in a variety of industrial and environmental applications like V/STOL engineering and film cooling of gas turbine blades. Specifically, the blades/vanes in gas turbines require proper cooling mechanism to protect the airfoils from thermal stresses generated by exposure to hot combustion gases. The problem becomes aggravated by the growing trend of using higher turbine inlet temperature to generate more power. Thus, film cooling is used as a cooling mechanism and it works in the form of row of holes in the spanwise directions of the blade, from where cold jet is issued into the hot crossflow. The mixing process during the penetration of the cold jet into the hot gas creates a three-dimensional complex flowfield. The resulting temperature downstream of the jet, the trajectory and physical path of the jet are critical design parameters. Systematic investigation of such flowfield started in late 50s. Figure 1 shows the schematic of a single round jet injected in the crossflow at an angle. This geometry has been extensively studied for cooling performance for a wide range of blowing ratios (i.e., momentum ratio of injected air to crossflow). These results show details of the vortex interaction region and mixing and mean centerline species concentration decay in the near and far field.

Goldstein[1] summarized early studies based on slot flows, and film cooling effectiveness values were found to correlate well with the parameter $x/Mb$, where $x$ is the downstream distance, M is the blowing ratio, and $b$ is the slot width. This parameter has also been used for discrete hole cooling, with $b$ defined as the effective slot width for the row of holes. However, the physics of discrete hole cooling is quite different from that of a slot. A row of discrete holes typically has a much lower span averaged downstream film effectiveness distribution for the same $x/Mb$. This may be due to the formation of vortices, which allow hot gas to penetrate to the wall. These vortices are of the scale of the hole size, so if a numerical simulation has a spanwise grid spacing greater than the film hole spanwise pitch, as is typical for turbine blade aerodynamic design, their effect is lost. In essence, any such calculation is two-dimensional on the scale of the film holes.

Sinha et al.[2] performed experimental studies on film cooling effectiveness using a row of inclined holes, through which cryogenically cooled air was injected into the hot crossflow to cool down an "adiabatic" surface. The results were obtained for different combinations of density ratio, velocity ratio, blowing ratio and momentum flux ratio. A number of experiments[3,4] were carried out to study the effect of density ratio on the hydrodynamics of the film cooling. Recently, a detailed experimental study was carried out by Yuen et al.[5], which discusses about the effect of geometrical (streamwise angles of $30^o$, $60^o$ and $90^o$) and fluid-thermal characteristics (M= 0.33 - 2) on the film cooling effectiveness for a single round hole. These results provide good comparison source for numerical results. Besides physical and fluid-thermal parameters, the characteristic of vortices originated at the trailing edge of the hole contributes a major part in film cooling performance. Lee et al.[6] carried out a detail experimental study on the effect of embedded vortices on film cooling performance for a row of 35 degree inclined holes and blowing ratio of 0.5. Numerical investigations of jets

[1] Graduate Research Assistant, Email: kapa9202@kettering.edu, AIAA Student member.
[2] Associate Professor, Email: sroy@kettering.edu, AIAA Associate Fellow
[3] Research Engineer, Email: james.heidmann@grc.nasa.gov, AIAA Member

based on integral methods were done by Vizel and Mostinskii[7] and Adler and Baron[8] using idealized models. A number of numerical models have been proposed that approximate the three-dimensional flow behavior with a two-dimensional one. However, the mixing of a jet in a cross-stream is a fully three-dimensional phenomenon[9] and thus, such idealized treatments lack accuracy. Numerical solutions of the full Navier-Stokes equations have been used to obtain detailed solutions in various studies. Early attempts by Chien and Schetz[10] used closure models based on constant turbulent viscosity. Amer et al.[11] pointed out that the flow predictions are greatly affected by the selection of the turbulence model. Later studies were based on the k-ε model of turbulence or its variants. These results indicate that the Reynolds averaged Navier-Stokes (RaNS) model gives predictions of engineering accuracy. Rai[12] used non-isotropic models, based on algebraic expressions for the Reynolds stresses. Roy[13] documented the cooling performance of twelve different arrangements of holes with a combination of blowing ratio M, distance between the holes L and jet angle α using a upwind biased finite volume code and standard k-ε turbulence closure model. Numerical solutions for these flow arrangements document strong to moderate secondary vortex structures spanning normal to the direction of the jet. This fully three-dimensional flow field strongly influences the cooling performance of the hole-blade system. Computational results predict an optimum hole spacing and low issuing angle for maximum cooling efficiency.

Several computational studies have computed turbine blade geometries with accurate resolution of the film holes, and in some cases, of the hole pipes and plena as well. Garg and Gaugler[14] showed the importance of film hole exit profiles. Garg and Rigby[15] resolved the plenum and hole pipes for a three-row showerhead film cooling arrangement with Wilcox's k-ω turbulence model. Heidmann et al.[16] used RaNS to compute the heat transfer for a realistic turbine vane with 12 rows of film cooling holes with shaped holes and plena resolved. Garg[17] presented results of a full rotating blade with 172 film holes, resolving the film hole exits, but not the hole pipes and plena. These studies provide good details of the flow.

In the near field of the film cooling jet, the dynamic large scale anisotropic structures control the mixing process[18]. This three-dimensional mixing determines the normal and transverse penetration of the jet. The accurate prediction of the jet penetration and reattachment location greatly influences the accuracy of the numerical prediction of the heat transfer process or the film cooling effectiveness on the adiabatic blade surface. The complex dynamic nature of the spanwise vortices makes it necessary to accurately model the flow field temporally and spatially using direct numerical simulation (DNS) or large eddy simulation (LES) of turbulence. Although, LES requires less computational effort or can simulate flows at higher Reynolds number than DNS, one major challenge for performing LES in film cooling is the range of length scales that must be resolved in the computation[19]. Several subgrid models exist in the literature. However, based on the scales, LES remains very expensive.

As a viable alternative, this paper presents the detached eddy simulation (DES) based modeling of film cooling flow for the three-dimensional geometry shown in Figure 1. DES is a hybrid turbulence model that works by applying a variable length scale that varies as a function of the distance to the nearest wall in the attached boundary layer and conforms with sub-grid scale in the rest of the flow including separated regions and near wake[20]. The literature indicates that the mixing processes downstream of the hole are highly anisotropic, as the turbulent diffusion is much stronger in the transverse direction (normal to the jet trajectory)

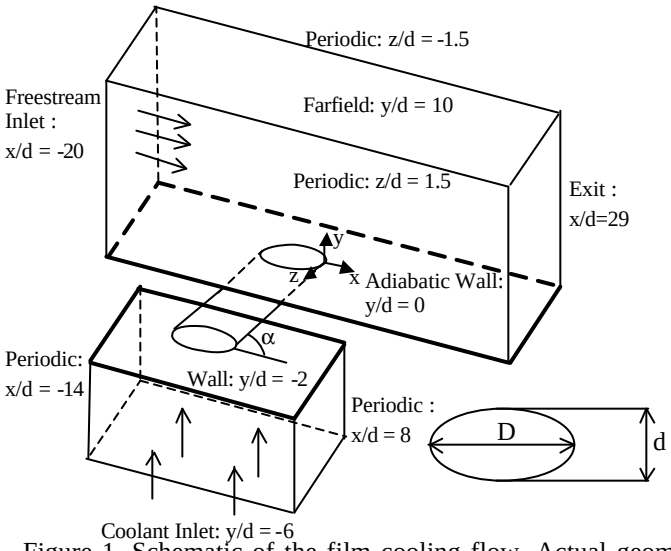

Figure 1. Schematic of the film cooling flow. Actual geometry definition and boundary conditions are based on Sinha et al[2].

than in the streamwise direction. This causes underprediction of jet spreading by the isotropic turbulence models like k-ω. The opportunity to utilize the DES simulations, which makes no such assumption of isotropy downstream of the hole, should enhance the modeling efforts by providing a more realistic description of the mixing processes on which the model will be based. Present work compares the values of centerline and spanwise effectiveness with the experimental values obtained by Sinha et al.[2] for blowing ratio 1, density ratio 2 and velocity ratio 0.5. The paper also documents comparison of DES and RaNS solution for blade-hole configuration.

**Nomenclature**

| | |
|---|---|
| $A, B, C$ | Viscous terms |
| b | Slot width |
| $C_{des}$ | Turbulence constant for S-A based DES model |
| $c$ | S-A constants |
| d | Hole diameter |
| $d_w$ | Distance to the nearest wall |
| $\vec{f}$ | flux vector |
| $F, G, H$ | flux vector components |
| $L$ | Distance between hole centers |
| M | Blowing ratio |
| $p$ | Pressure |
| q | State variable |
| Re | Reynolds Number |
| $\tilde{S}$ | Production term |
| S | Value of vorticity |
| $T$ | Static temperature of the blade |

$T_{fs}$ Hot freestream temperature

$T_j$ Cool jet temperature

$u_{fs}$ Freestream velocity

$u$ X-component of the velocity

$v$ Y-component of the velocity

$w$ Z-component of the velocity

$V$ Fluid element volume

$\Delta x_i$ Mesh size in respective cartesian directions

$y^+$ Inner variable

*Greek*

$\alpha$ Jet issuing angle

$\delta$ Fluid element surface area

$\Delta$ Grid spacing

$\phi$ S-A functions

$h$ Film cooling effectiveness, $\left(T_{fs}-T\right)/\left(T_{fs}-T_j\right)$

$n$ Molecular viscosity

$n_T$ Turbulence kinematic viscosity

$\tilde{n}$ Working variable

$n^*$ Reference turbulent kinematic viscosity

$r$ Density

$\theta$ Implicitness

**TURBULENCE MODEL**

The complex dynamic nature of the film cooling flow makes it necessary to model the vortices using temporally and spatially accurate calculation of the flow field to capture the dominant turbulence length scales. Various turbulence models are available in the literature[21,22]. The two competing factors important for any turbulence model are accuracy and efficiency (i.e. computational cost). An optimal combination of both these factors is hard to achieve and thus, the primary purpose of the numerical simulation is towards attaining such a goal. Numerical simulations in this study were performed using a finite volume based parallel, implicit, unstructured Euler/Navier-Stokes flow solver called Cobalt[23,24].

**RaNS, LES and DNS modeling**

A brief discussion on available turbulence modeling techniques in terms of accuracy and computational cost is presented in this section.

Of all the available turbulence models, DNS explicitly accounts for all scales of motion in a turbulent flow, from the largest, imposed by the existence of boundaries or periodicities, to the smallest. Kim et al.[25] showed that DNS for fully developed incompressible channel flow at a Re of about 6000 (based on channel height) requires grid with 2 and 4 million points. Wilcox[26] gave the following equation to estimate the number of required grid points for DNS channel flow.

$$N_{DNS} = (0.088 Re_h)^{9/4} \quad (1)$$

where $Re_h$ is the Reynolds number based on the mean channel velocity and channel height. This imposes critical limitation on the applicability of DNS for practical high Reynolds number flows using present day computers.

Another expensive closure model used to resolve unsteady turbulent flows is LES[27,28], in which large-scale structure of turbulent flow is computed directly and the smallest and nearly isotropic eddies are modeled as sub-grid length-scales. Moin[28] has described numerical and physical issues involved in LES. Ghosal[29] concluded that explicitly filtered space averaged equations give satisfactory results with finite difference if filter width is larger than the cell size in the computational grid. Computational requirement for LES is approximately $(1/10)^{th}$ times of that of DNS.

In the low end of accuracy, RaNS is considered as the most practical turbulence handling technique with the present day available computational resources. The Reynolds equations are derived by decomposing the dependent variables of Navier-Stokes conservation equations into time-mean and fluctuating components and then time averaging the entire equation. As equations are averaged in this technique, additional assumptions are required to close the system of equations, which forms the basis of RaNS turbulence modeling. This technique can be further classified and the most common classification is based on the number of supplementary partial differential equations e.g. two equation k-ε model that must be solved in order to supply the modeling parameters.

Evidently each turbulence model has its own benefits and drawbacks. Proposed by Spalart et al.[30], DES is a hybrid model which combines the computational efficiency of RaNS and the numerical accuracy of LES length scales to work under a single turbulence framework. Two different DES models[20,31] are currently available in the numerical code used in the present simulation:

(1) S-A (Spalart-Allmaras) based DES model,
(2) M-SST (Menter's shear stress transport) based DES model.

Spalart-Allmaras based DES model is used in the present study.

**Spalart-Allmaras (S-A) model**

Spalart-Allmaras[32] is a one equation RaNS model, which is used in the present simulation. The S-A model solves a single partial differential equation for $\tilde{n}$, which is related to the turbulent viscosity. The model employs a transport equation for the turbulent viscosity using empirical and dimensional analysis, Galilean invariance and selected dependence on molecular viscosity. It includes a wall destruction term to reduce the turbulent viscosity in the log layer and laminar sublayer. The model also uses trip terms for transition between laminar and turbulent flow.

The following transport equation is used to calculate $\tilde{n}$.

$$\frac{D\tilde{n}}{Dt} = c_{b1}[1-f_{t2}]\tilde{S}\tilde{n} - \left[c_{w1}f_w - \frac{c_{b1}}{k^2}f_{t2}\right]\left[\frac{\tilde{n}}{d_w}\right]^2 + \frac{1}{s}\left[\nabla.((n+\tilde{n})\nabla\tilde{n}) + c_{b2}(\nabla\tilde{n})^2\right] + f_{t1}\Delta U^2 \quad (2)$$

The SA turbulent kinematic viscosity is given by,

$$n_T = \tilde{n} f_{v1} \tag{3}$$

Eddy viscosity can be found out by using (2) and (3). Constants and functions in (2) and (3) can be defined as follows:

$$f_{v1} = \frac{c^3}{c^3 + c_{v1}^3}, \qquad c \equiv \frac{\tilde{n}}{n} \tag{4}$$

$\tilde{S}$ is a production term and can be expressed as,

$$\tilde{S} = f_{v3} S + \frac{\tilde{n}}{k^2 d_w^2} f_{v2}, \tag{5}$$

where S is the magnitude of the vorticity and functions

$$f_{v2} = \left[1 + \frac{c}{c_{v2}}\right]^{-3}, \tag{6}$$

$$f_{v3} = \frac{(1 + c f_{v1})(1 - f_{v2})}{c}, \tag{7}$$

Note that the production term in (5) is different from that developed by Spalart and Allmaras.[32] This is due to the different form of $f_{v2}$ and inclusion of a new term $f_{v3}$. Now,

$$f_w = g\left[\frac{1 + c_{w3}^6}{g^6 + c_{w3}^6}\right]^{1/6}, \tag{8}$$

where, $g = r + c_{w2}(r^6 - r), \quad r \equiv \frac{\tilde{n}}{\tilde{S} k^2 d_w^2}.$ (9)

Trip terms $f_{t1}$ and $f_{t2}$ are defined as,

$$f_{t1} = c_{t1} g_t \exp\left(-c_{t2} \frac{w_t^2}{\Delta U^2}\left[d_w^2 + g_t^2 d_t^2\right]\right) \tag{10}$$

$$f_{t2} = c_{t3} \exp(-c_{t4} c^2). \tag{11}$$

where, $d_t$ is the distance from the field point to the trip layer, $\omega_t$ is the wall vorticity at the trip and $\Delta U$ is the difference between the velocity at the field point and that at the trip.

$g_t = \min(0.1, \Delta U / w_t \Delta x)$, where $\Delta x$ is the grid spacing along the wall at the trip.

Following constants are used in equation (2) to (11).

$c_{b1} = 0.1355,\ c_{b2} = 0.622,\ s = 2/3,\ k = 0.41,$

$c_{w1} = \frac{c_{b1}}{k^2} + \frac{1 + c_{b2}}{s},\ c_{w2} = 0.3,\ c_{w3} = 2,$

$c_{v1} = 7.1,\ c_{v2} = 5,\ c_{t1} = 1,\ c_{t2} = 2,\ c_{t3} = 1.1,\ c_{t4} = 2.$

Trip terms are not used in the simulation presented in this paper. Thus, transport equation (2) takes the following form for the case presented in this paper.

$$\frac{D\tilde{n}}{Dt} = c_{b1} S \tilde{n} - c_{w1} f_w \left[\frac{\tilde{n}}{d_w}\right]^2 + \frac{1}{s}\left[\nabla.((n + \tilde{n})\nabla\tilde{n}) + c_{b2}(\nabla\tilde{n})^2\right] \tag{12}$$

**Detached Eddy Simulation**

Present definition of DES, as described by Strelets[20], is a three-dimensional unsteady numerical tool using a single turbulence model, which works as a subgrid-scale model in regions where grid density is fine enough for an LES, and as a RaNS elsewhere. RaNS is considered as an adequate and reliable technique to predict the flow in thin shear layers and LES has already proven to be powerful to predict the flow in large separated zones. Further, progress of unsteady RaNS (URaNS) in achieving accuracy is not much encouraging. Thus, DES combines LES and RaNS in such a way that RaNS technique can be used for the flow in thin shear layers and LES can be used for large separated zones for resolution of geometry-dependent and three-dimensional eddies.

In S-A based DES formulation, distance to the nearest wall, $d_w$ is replaced by $\tilde{d}$,

$$\tilde{d} = \min(d_w, C_{DES}\Delta) \tag{13}$$

where, $C_{DES}$=0.65 and $\Delta = \max(\Delta x, \Delta y, \Delta z)$ is the largest distance between the cell center under consideration and the cell center of the neighbors.

Equation (13) keeps the DES model within RaNS model inside the whole attached boundary layer as streamwise or spanwise or both grid spacing parallel to the wall are at least of the order of the boundary layer thickness. Thus, in (13), $\tilde{d} = d_w$ and model works as a standard S-A turbulence model inside the boundary layer and the prediction of the boundary layer separation is also made by RaNS mode of DES. In the regions, far from the wall, where $d_w > C_{des}\Delta$, the length scale of the model becomes grid-dependent. The model performs as a subgrid-scale version of the S-A model for eddy viscosity. When production and destruction terms balance each other, this model reduces to an algebraic mixing-length Smargorinski-like subgrid model. Recently, Forsythe et al.[33] and Kapadia et al.[34] have successfully implemented DES for external flow simulation over a fighter aircraft and an Ahmed reference car, respectively.

## NUMERICAL METHOD

**Algorithm**

Present study implements Cobalt[23,24], a parallel, implicit, unstructured finite-volume based flow solver that uses second-order accurate spatial and temporal Godunov schemes.[35] The cell-centered finite volume approach is used in the computational method. Hansen and Forsythe[36] validated the ability of the second order accurate discretization of the present unstructured solver to work in the LES mode. The dynamics evolution is an implicit procedure and the size of the time-step is a function of CFL condition. Initial value of CFL number is taken as $10^3$, which gradually increases to $10^6$ after 130 timesteps and remains constant thereon. Size of the timestep at the final CFL number is 6.17 x $10^{-4}$s. The grid is divided into groups of cells, or zones, for parallel processing.

Five fundamental tasks comprise the flow solution algorithm: Construction of initial conditions for the Riemann problem at any given face, solution of this Riemann problem, construction of viscous fluxes at any given face, time integration, and boundary conditions. The first step, constructing the initial conditions for the Riemann problem, is critical to the algorithm, for it includes any limiter or dissipation and it largely determines the spatial accuracy and truncation error of the scheme.

The baseline RaNS calculations were performed using the NASA Glenn-HT code. These results were previously described by Heidmann and Hunter[37]. Briefly, the code solved the full

compressible Reynolds-averaged Navier-Stokes equations. It also employed the finite volume method with central differencing. The k-ω turbulence model was used without wall functions, as the computational grid was sufficiently fine to yield y+ values of less than 1.0 at the first cell from the wall.

Data distribution is assumed to be linear in each cell. Equation used for Riemann problem to find out the left initial state for face $J$ of cell $i$ is,

$$q_i^J = q_i + \vec{r}_i^{\,J} . \vec{\nabla} q_i \tag{14}$$

$q_i^J$ is the estimated value at the centroid of face $J$ due to cell *i*, $\vec{\nabla} q_i$ is the gradient vector and $\vec{r}_i^{\,J}$ is a vector from the centroid of the cell i and pointing towards the centroid of face $J$. The gradient vector for cell $i$ is found by a least-squares solution to (14). Right initial state for face *J* can be found in the similar way.

Final equation in the matrix form after considering the nearest-neighbor cells is,

$$A\vec{\nabla}^c q_i = \{q_m - q_i\} \tag{15}$$

where, $\vec{\nabla}^c q_i$ is a central difference gradient and A is an over-determined matrix due to more number of nearest-neighbor cells (equations) than unknowns. Eq. (15) is solved by QR factorization. Following equation shows the temporal integration used in the numerical scheme.

$$q\left\{V\frac{dq}{dt} + \vec{\nabla}.\vec{f}\right\}_i^{n+1} + (1-q)\left\{V\frac{dq}{dt} + \vec{\nabla}.\vec{f}\right\}_i^{n} = 0 \tag{16}$$

where, θ is the implicitness, $\vec{f}$ is a flux vector, n and (n+1) shows successive time-steps.

Temporal derivatives in the discrete form for $n^{th}$ and $(n+1)^{th}$ time-steps are as follows:

$$\left(\frac{\partial q}{\partial t}\right)^{n+1} = \frac{a_{1,1}(q^{n+1} - q^n) + a_{1,2}(q^n - q^{n-1})}{\Delta t} \tag{17}$$

$$\left(\frac{\partial q}{\partial t}\right)^{n} = \frac{a_{2,1}(q^{n+1} - q^n) + a_{2,2}(q^n - q^{n-1})}{\Delta t} \tag{18}$$

where, $\alpha_{1,1} = 3/2$, $\alpha_{1,2} = (-1/2)$, $\alpha_{2,1} = \alpha_{2,2} = 1/2$ for second-order accuracy. Finally, the semi-discrete form of the governing equation is given by,

$$V_i\frac{dq_i}{dt} + \sum_{M=1}^{N_i}\left(F^M\hat{i} + G^M\hat{j} + H^M\hat{k}\right)\hat{n}^M d^M = \sum_{M=1}^{N_i}\left(A^M\hat{i} + B^M\hat{j} + C^M\hat{k}\right)\hat{n}^M d^M \tag{19}$$

where the subscript *i* and superscript M denote quantities for the $i^{th}$ cell and the $M^{th}$ face of cell *i*, respectively, and $N_i$ is the number of faces bounding cell *i*.

**Grid information and Computational approach**

It is easy to appreciate the geometric complexity of realistic turbine blades as analyzed by Garg and Rigby[15]. In this paper, a simplified plate is used to verify the capability of DES in capturing the dynamic details of the spanwise mixing process. There is a relatively large body of experimental data for a row of 35 deg.-pitch round holes on a flat plate with a spacing 3d[2,37]. This geometry allows for a study of jet lift-off behavior at various blowing ratios and is perhaps the most realistic simplified geometry for turbine film cooling. In addition, the computational study of Heidmann and Hunter[37] and the experimental data of Sinha et al.[2] use this geometry and give an excellent scope for DES solution validation in this geometry.

The multi-block computational grid was initially developed using GridPro multiples grid generator with 15 blocks and approximately 2,600,000 computational cells. Gridgn14.03 is then used to convert this grid into Cobalt compatible unstructured grid. The final mesh used in this solution contains a single block of 2109440 cells. Viscous clustering was employed at all solid walls with a $y^+$ value less than 1.0 at all locations. Stretching ratios less than 1.2 were used normal to the viscous walls. Iteration convergence was considered achieved when all residuals reduce by four orders of magnitude.

Present case is run on the cluster of 64 parallel processors on Blue Horizon supercomputer at SDSC. The aggregate CPU time requirement for the entire DES solution is 37.46 seconds/iteration and that for one cell is 17.76 micro seconds/iteration. The aggregate CPU time includes flow solution time, problem set-up time and restart file creation time. The presented case has been run for 6000 time-steps and corresponding real time of the solution is 3.7 seconds. Total CPU requirement for this solution is approximately 4000 hours.

**RESULTS AND DISCUSSION**

Figure 1 describes schematic control volume of hot air passing over an adiabatic flat surface (e.g., a turbine blade). The surface of study has a row of injection holes through which cool air at temperature $T_j$ =150K is injected at an angle α=35° into the hot freestream of $T_{fs}$ =300K. The injection ducts are circulars with diameter equal to d=2.54mm. The injection cross-section formed by the intersection of the injection pipe with the wind tunnel is an ellipse with the minor and the major axes d and D=d/(sin α), respectively. The distance between the hole centers is L=3d. The selected mean flow velocities, static pressures and temperatures (i.e., densities) in the injection pipe and the wind tunnel gives a blowing ratio M=1, density ratio = 2 and velocity ratio = 0.5. The inlet section (trailing edge of the hole) is located at x=-20d and the exit at x=29d. The other dimensions and boundary conditions are shown in Figure 1.

Periodic boundary conditions are employed in the spanwise direction and on all sides of the plenum. Farfield boundary condition is applied at the y/d=10 plane. Even though use of symmetry boundary condition at the hole centerline would reduce the computational time by half, it is avoided to capture the unsteady asymmetric vortical flow patterns. The large scale structures convecting downstream may induce these three-dimensional instability waves. At the plenum and freestream, fixed mass flow rate and stagnation temperature inlet boundary conditions are used to ensure proper density and blowing ratios. Flows were normal to the inlet. Adiabatic no-slip conditions are applied at all solid walls, including the inner surface of the film

hole and the plenum. The Reynolds number based on hole diameter and inlet conditions is 19700. An exit boundary condition with fixed static pressure is employed at x/d=29. The maximum Mach number not exceeding 0.3 is achieved in the flow field. Results described in this section correspond to the time-averaged DES solution after 3.7s, when solution reaches quasi-stationary state.

Figure 2(a) shows the speed contours at the center plane (z=0). It is evident that in the right half, the entrained fluid creates a small recirculation zone. Velocity vectors in this region are shown in Figure 2(b). Especially at the exit plane of the tube, the flow is highly non-uniform. This is in qualitative agreement with the results of Heidmann and Hunter[37]. Average normal velocity of the fluid at the hole exit is 52 m/s, which maintains the velocity ratio of 0.5. Clearly, for this moderate blowing ratio of M=1 and a combination of flow profiles at the wind tunnel and cold jet inlet, the effect of the vorticity in the pipe is not negligible, which is also evident from the Figure. This is due to the fact that at this range of velocities in the pipe, the boundary layers are not thin everywhere in the pipe.

Heidmann and Hunter[37] pointed out that a more realistic description of the coolant boundary layer profile is needed in conjunction with downstream entrainment models to resolve the effect of the downstream vortices. DES presents that opportunity of realistic boundary layer description. Figure 3 shows the interface between RANS and LES region, where $d_w = C_{des}\Delta$. It is evident from the figure that DES predicted boundary layer has the starting point at the trailing edge of the hole and thus, treatment of the most complicated process - initial penetration of jet into freestream is carried out by pure LES technique. The reason is that mesh size in the streamwise direction ($\Delta$) at and just above the hole exit is smaller than the wall distance ($d_w$).

Figure 4 shows velocity vector distribution in the spanwise direction at x= 5d plane. The figure clearly shows the presence of instability in the flow and the ability of DES to capture the asymmetric bound vortices. The assumption of uniform u-velocity profile in the wind tunnel leads to higher *v*-values in the near-jet downstream region. The tendency is that as the boundary layer in the wind tunnel becomes thicker, the velocity maxima appear at higher distances from the wall and the near-wall flow changes dramatically.

For better understanding of the simulations, flowfield can be divided into three areas: (i) The central jet, (ii) the near jet and (iii) the wake region. The jets coming out of the pipes appear to the crossflow as "solid". A sharp velocity and temperature gradient is formed at the time cold jet penetrates into the hot main flow near hole exit and "wake" region develops downstream of the jet. In the latter a pair of bound vortices per jet is formed, which bends the jet, producing the well-known kidney shape both in speed and temperature line contours.

Figure 5 shows two iso-surfaces of z-vorticity. The values of the z-vorticity for the left and right iso-surfaces are -10000 $s^{-1}$ and 10000 $s^{-1}$ respectively. Both iso-surfaces are colored by temperature. Figure clearly indicates that the maximum recirculation is present at the location where cold jet hits the hot crossflow and the pattern is highly non-uniform. While in the wake region, recirculation follows uniform pattern of a pair of counter-rotating vortices, described in the Figure 4. The red color shows the temperature of 300 K and blue color shows the temperature of 150 K. It is evident that sharp temperature gradient is present at the time of mixing process and temperature distribution looks more diffused in the wake region.

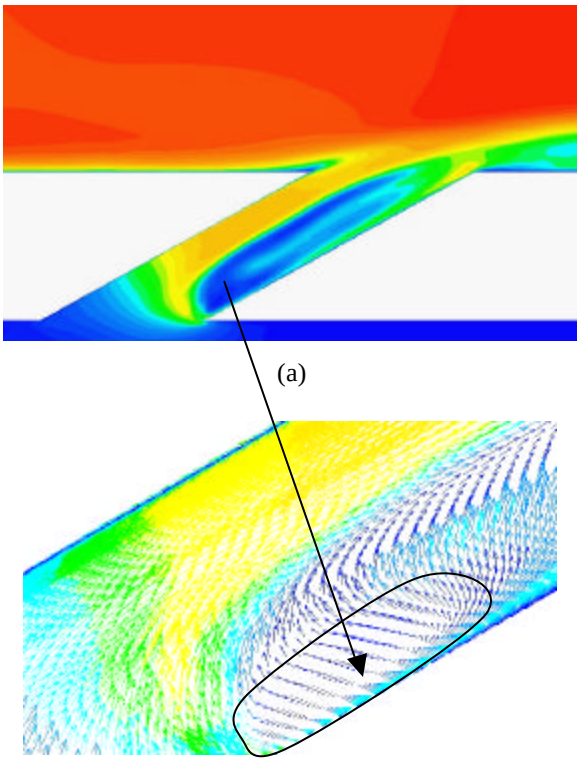


Figure 2. Time-averaged DES solution at z= 0 surface after 3.7s shows (a) speed contours and (b) velocity vectors (recirculation zone inside the tube).

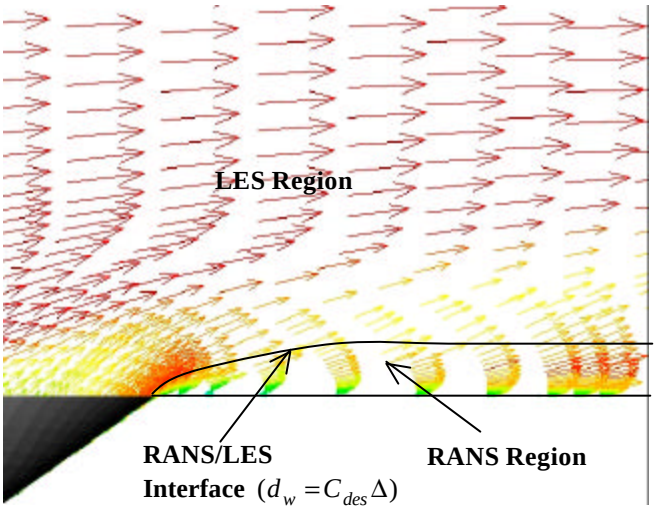


Figure 3. Comparison between numerically predicted boundary layer (DES/RANS interface) and actual boundary layer (velocity vectors colored by u-velocity).

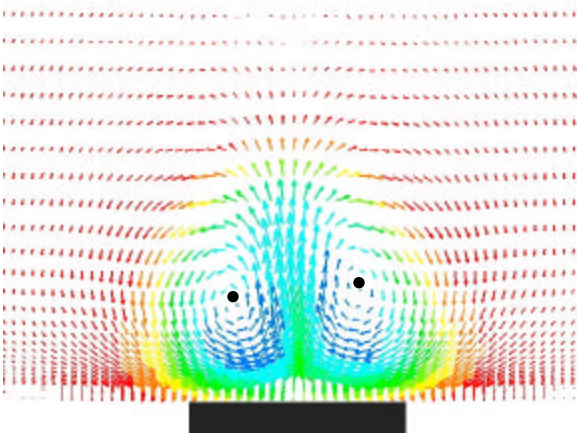

Figure 4. Velocity vectors colored by temperature at x/d = 5 after 3.7sec (Time-averaged solution) shows a pair of counter-rotating vortices.

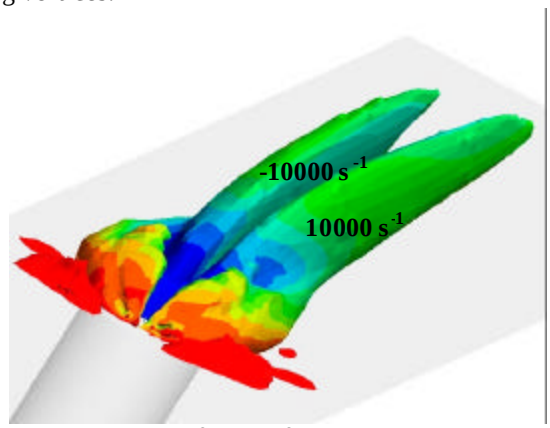


Figure 5. Two Iso-surfaces of x-vorticity (-10K and 10K) colored by the temperature.

Since the DES solution is inherently unsteady and involves fluctuating components, it is important to run the simulation to a quasi-stationary state where the solution does not evolve beyond a preset criteria. For the present problem, the solution reaches such a state beyond 3.7s. Figures 6 documents the time history of numerically calculated mass flux at the hole exit (y=0). The inset clearly shows the unsteady nature of the flow. In order to compare DES results with a RaNS solution, it is crucial that one determines the time-averaged data for DES.

Blade temperature prediction is the primary interest for film cooling analysis. Figures 7(a) and (b) shows qualitative comparison of the temperature distribution on the blade surface for RaNS and DES solution respectively. Figure 7(c) plots the normalized temperature line contours for the same DES solution quantitatively. Figure clearly shows that maximum cooling (0.73) takes place in a very small region just beyond the trailing edge of the hole (less than 1d in streamwise direction), which is similar to the experimental results obtained by Sinha et al.[2]. Downstream, beginning at approximately 6d in streamwise direction, the blade temperature reduces (0.78) and remains cool for nearly 7d. One significant feature of DES is that one sees very little spanwise diffusion.

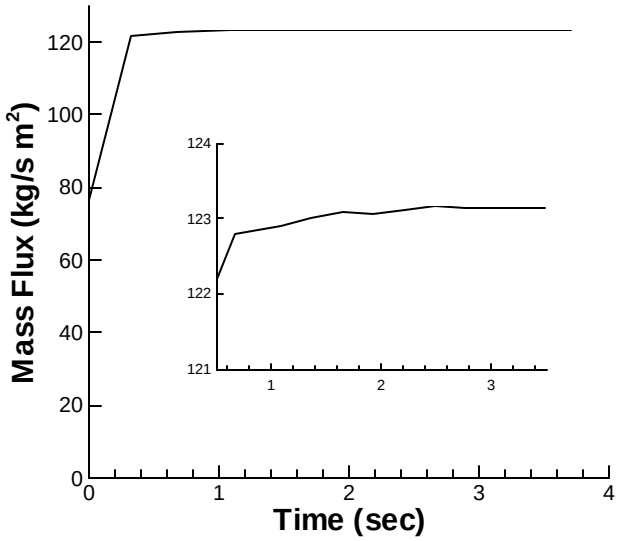


Figure 6. Time history of the mass flux at the hole exit.

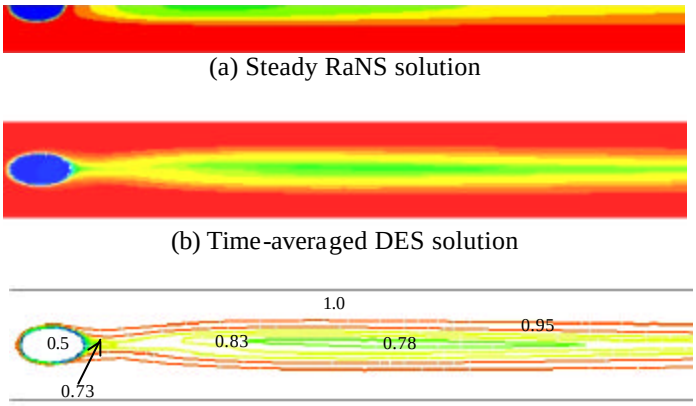


(a) Steady RaNS solution

(b) Time-averaged DES solution

(c) Temperature contour lines for DES time-averaged solution

Figure 7. Comparison of temperature distribution for RaNS and DES solution on the flat plate (y/d=0).

Since film cooling is a strongly coupled fluid-thermal process, the effect of flow structures on fluid temperature distribution is plotted at x=3.5d in Figures 8(a) and (b). While Figure 8(a) plots the RaNS solution at steady state, Figure 8(b) shows the quasi-stationary and time-averaged DES results on the same plane. The RaNS solution in Figure 8(a) is quite diffused as is evident from the temperature contours. In comparison, DES time-averaged data shows prominent features of elongated kidney-shaped bound vortex followed by similar temperature profiles. Presence of asymmetry can be observed in the DES solution of both velocity vectors and temperature profile. Temperature is normalized by the hot crossflow temperature (300K). The coolest flow region is located at just below the vortex center for both RaNS and DES solutions.

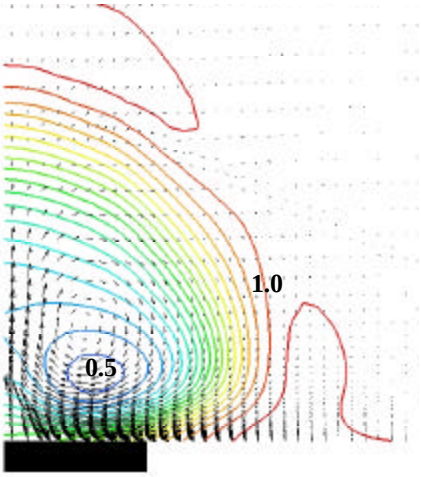


Figure 8(a). Steady RaNS solution velocity vectors with superimposed temperature contour lines at x/d = 3.5.

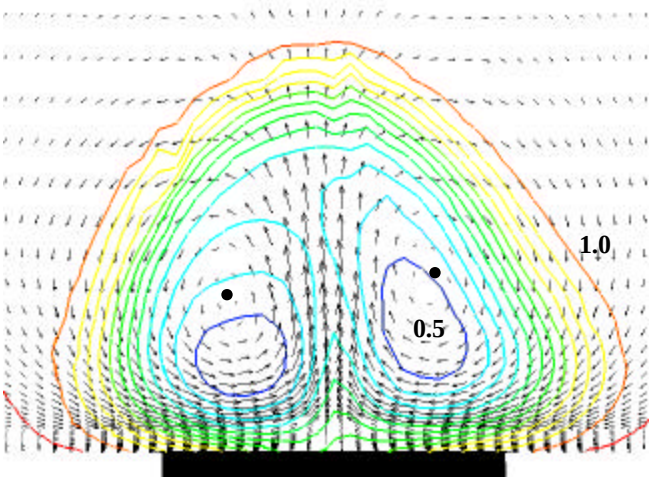


Figure 8(b). Velocity vectors with superimposed temperature contour lines at x/d = 3.5 for time -averaged DES solution

Figure 9 exhibits various fluid thermal characteristics of the flowfield. Complex nature of the flow inside the pipe can be observed from the twisted shape of the streamlines inside the pipe. As the x-component of the velocity is prominent, it is hard to observe the bending of the jet towards the blade surface after its interaction with the main flow by looking at the streamlines. Five different x-planes, x=1d, 3d, 6d, 10d and 15d, are shown in the figure. These planes alongwith the blade surface are colored by the temperature. From the kidney-shaped temperature contours at different x-planes, one can easily observe the presence of a pair of counter-rotating vortices, which is asymmetric and the center of the vortex is moving away from the blade surface as the flow moves downstream. It is clearly shown in Figure 9 that solution is highly asymmetric for the film cooling problem and thus, assumption of the symmetry (like in RaNS) would not be accurate to capture the essential fluid thermal characteristics of the flow.

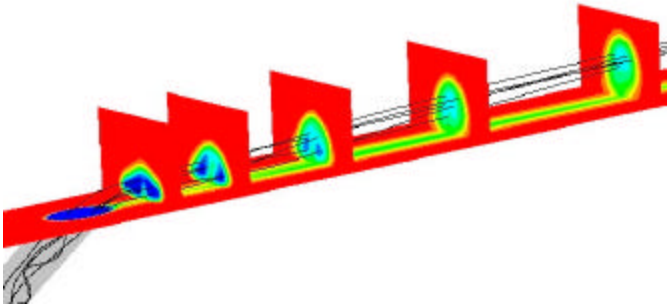

Figure 9. Temperature distribution (at x/d =1,3,6,10,15) and streamlines shows asymmetry in the DES solution.

Comparison between experimental[2] and numerical (time-averaged DES) values of centerline and span-averaged effectiveness is shown in Figures 10 (a) and (b), respectively. The sharp difference between the experimental and the numerical results for centerline effectiveness at x = 1d stems from the fact that although in the numerical prediction of maximum cooling occurs near the trailing edge of the hole (similar to the experimental data), its streamwise length is less than 1d (see Fig. 7c). For both centerline and span-averaged effectiveness, experimental and numerical results show close similarity between x=1d to x = 6d. For experimental results, centerline effectiveness starts reducing beyond this point, while spanwise effectiveness keeps on increasing upto 15d (experimental span-averaged effectiveness values are available upto 15d only). Interestingly beyond x=6d, numerical values of centerline effectiveness are higher than the experimental values. Further, at these points, numerical values of span-averaged effectiveness are lower than that of experimental results. Though Sinha et al.[2] described their experimental results as conduction error corrected, these differing trends between experimental and numerical values suggest the presence of conduction in experimental data. Figures 11(a), (b) clearly document very little diffusion in the spanwise direction for numerical solution at x=10d and x = 15d. This results in smaller values of span-averaged effectiveness in the numerical solution despite having higher centerline effectiveness.

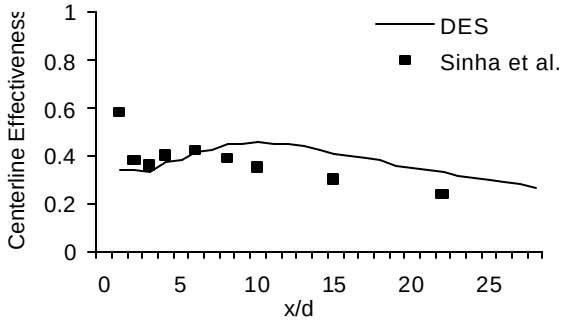


Figure 10(a). Comparison between experimental and numerical (Time-averaged DES) values of centerline effectiveness.

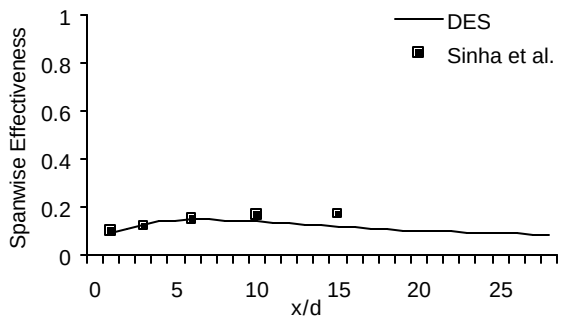


Figure 10(b). Comparison between experimental and numerical (Time-averaged DES) values of span-averaged effectiveness

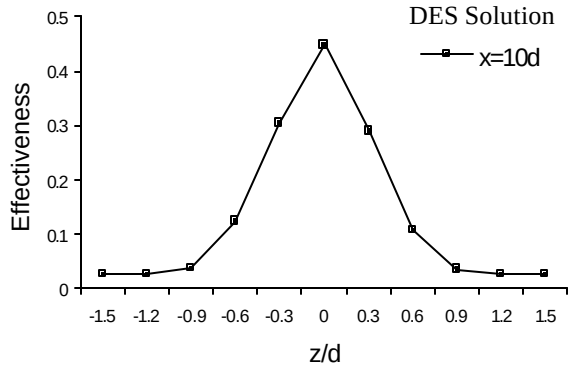


Figure 11(a). Spanwise distribution of effectiveness (x=10d).

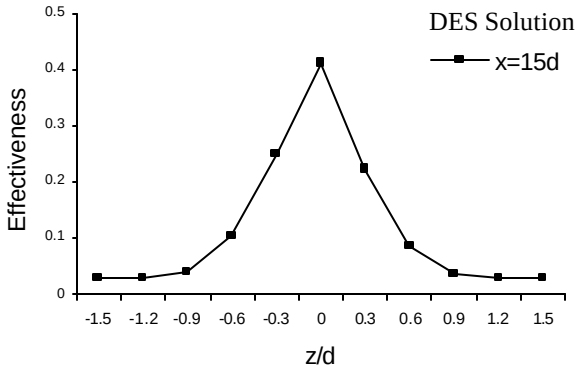


Figure 11(b). Spanwise distribution of effectiveness (x=15d).

## CONCLUSION

The first detached eddy simulation of film cooling has been presented for a widely published blade-pipe configuration. The blowing ratio was unity and density ratio was two. Results indicate that the mixing processes downstream of the hole are highly anisotropic. DES time-averaged solution clearly shows its ability to closely depict the dynamic nature of the flow. Further, comparison between experimental and DES time-averaged effectiveness is satisfactory. Though numerical values of centerline and span-averaged effectiveness differs from that of experimental values at downstream locations, one can justify it by indicating the possibility of conduction errors present in the experiment. Numerical prediction for effectiveness clearly looks less diffused than indicated in experimental data. In comparison to the reported RaNS solution, which uses symmetry boundary condition, DES solution looks more realistic as it captures the asymmetry present in temperature and velocity distribution.

## ACKNOWLEDGMENTS

This research was supported in part by NASA Grant no. NAG3-2843 and NSF cooperative agreement ACI-9619020 through computing resources provided by the National Partnership for Advanced Computational Infrastructure at the San Diego Supercomputer Center.

## REFERENCES

[1]Goldstein, R. J., "Film Cooling, Advances in Heat Transfer", Vol. 7, Academic press, New York, pp. 321-379, 1971.
[2]Sinha, A. K., Bogard, D. G. and Crawford, M. E., "Film-Cooling Effectiveness Downstream of a Single Row of Holes With Variable Density Ratio", J. Turbomachinery, 113, pp. 442-449, 1991.
[3]Pietrzyk, J. R., Bogard, D. G. and Crawford, M. E., "Effects of Density Ratio on the Hydrodynamics of Film Cooling", J. Turbomachinery, Vol. 112, pp. 437-443, 1990.
[4]Ito, S., Goldstein, R. J. and Eckert, E. R. G., "Film Cooling of a Gas Turbine Blade", Transactions of the ASME, J. Engineering for Power, 100, pp. 476-481, 1978.
[5]Yuen, C. H. N. and Martinez-Botas, R. F., "Film cooling characteristics of a single round hole at various streamwise angles in a crossflow: Part I effectiveness", Int. J. Heat and Mass Transfer, 46, 2002.
[6]Lee, J. S., Jung, H. G. and Kang, S. B., "Effect of embedded vortices on film cooling performance on a flat plate", Experimental and Thermal Fluid Science, 26, pp. 197-204, 2002.
[7]Vizel, Y. M. and Mostinskii, I. L., "Deflection of a jet injected into a stream", *Fluid Dynamics*, 8, pp. 127-139, 1965.
[8]Adler, D. and Baron, A., "Prediction of a three-dimensional circular turbulent jet in a crossflow", *AIAA Journal*, 17, pp. 168-174, 1979.
[9]Fric, T. F. and Rosko, A., "Vortical structure in the wake of a transverse jet", *J. Fluid Mechanics*, 279, pp. 1-47, 1994.
[10]Chien J. C. and Schetz, J. A., Numerical solution of the three dimensional Navier-Stokes equations with applications to channel flows and a buoyant jet in a cross flow", *ASME J. Appl. Mech.*, 42, pp. 575-579, 1975.
[11]Amer, B., Jubran, A. and Hamdan, M. A., "Comparison of different two-equation turbulence models for prediction of film cooling from two rows of holes", *Numerical Heat Transfer, Part A*, 21, pp. 143-162, 1992.
[12]Rai, M. M., "Navier-Stokes simulations of blade-vortex interaction using high-order accurate upwind schemes", *AIAA Paper 87-0543*, 1987.
[13]Roy, S., "Numerical Investigation of the Blade Cooling Effect by Multiple Jets Issuing at an angle", *J. Num. Heat Transfer*, 38, no. 7, pp. 701-718, 2000.
[14]Garg, V. K. and Gaugler, R. E., "Effect of Velocity and Temperature Distribution at the Hole Exit on Film Cooling of Turbine Blades", J. Turbomachinery, 119, pp. 343-351, 1997.
[15]Garg, V. K. and Rigby, D. L., "Heat Transfer on a Film-Cooled Blade - Effect of Hole Physics", Int. J. Heat and Fluid Flow, 20, pp.10-25, 1999.
[16]Heidmann, J. D., Rigby, D. L. and Ameri, A. A., "A Three-Dimensional Coupled Internal/External Simulation of a Film-

Cooled Turbine Vane", J. Turbomachinery, 122, pp. 348-359, 2000.
[17]Garg, V. K., "Heat Transfer on a Film-Cooled Rotating Blade", Int. J. Heat and Fluid Flow, 21, pp. 134-145, 2000.
[18]Ho, C.M. and Huerre, P., "Perturbed Free Shear Layers", *Ann. Rev. Fluid Mech*., 16, pp. 365-424, 1984.
[19]Lesieur, M., Comte, P., Lamballais, E., Métais, O. and Silvestrini, G., "Large-eddy simulations of shear flows", J. *Eng. Math.* ,32, pp. 195-215, 1997.
[20]Strelets, M., "Detached Eddy Simulation of Massively Separated Flows", AIAA Paper 01-0879, 2001.
[21]Pope, S. B., "Turbulent Flows", Cambridge University Press, Cambridge, United Kingdom, 2000.
[22]Spalart, P. R., "Trends In Turbulence Treatment", AIAA Paper 00-2306, 2000.
[23]Grismer, M. J., Strang, W. Z., Tomaro, R. F. and Witzeman, F. C., "Cobalt: A parallel, implicit, unstructured Euler/Navier-Stokes solver", Advances in Engineering Software, 29, 3-6, 365-373, 1998.
[24]Strang, W. Z., Tomaro, R. F. and Grismer, M. J., "The Defining Methods of $Cobalt_{60}$ : A Parallel, Implicit, Unstructured Euler/Navier-Stokes Flow Solver", AIAA Paper 99-16635, 1999.
[25]Kim, J., Moin, P. and Moser, R., "Turbulence Statistics in Fully Developed Channel Flow at Low Reynolds Number", J. Fluid Mech. 177, 133-166, 1987.
[26]Wilcox, D. C., "Turbulence Modeling for CFD", DCW Industries, La Canada, California, 1993.
[27]Ansari, A. and Strang, W. Z., "Large-eddy simulation of turbulent mixing layers", AIAA Paper 96-0684, 1996.
[28]Moin, P., "Numerical and Physical Issues in Large Eddy Simulation of Turbulent Flows", JSME International Journal, 41, 2, 1998.
[29]Ghosal, S., "An analysis of numerical errors in Large Eddy Simulation of Turbulence", J. Comp. Phys., 125, pp. 187-206, 1996.
[30]Spalart, P. R., Jou. W-H., Strelets, M. and Allmaras, S. R., "Comments on the Feasibility of LES for Wings, and on a Hybrid RaNS/LES Approach", Advances in DNS/LES, 1st AFOSR Int. Conf. on DNS/LES, Aug 4-8, Greyden Press, Columbus, Ohio, 1997.
[31]Squires, K. D., Forsythe, J. R., Morton, S. A., Strang, W. Z., Wurtzler, K. E., Tomaro, R. F., Grismer, M. J. and Spalart, P. R., "Progress on Detached-Eddy Simulation of Massively Separated Flows", AIAA Paper 02-1021, 2002.
[32]Spalart, P. R. and Allmaras, S. R., "A One-Equation Turbulence Model for Aerodynamic Flows", AIAA Paper 92-0439, 1992.
[33]Forsythe, J. R., Squires, K. D., Wurtzler, K. E. and Spalart, P. M., "Detached-Eddy Simulation of Fighter Aircraft at High Alpha", AIAA Paper 02-0591, 2002.
[34]Kapadia, S., Roy, S. and Wurtzler, K., "Detached Eddy Simulation Over a Reference Ahmed Car Model", AIAA Paper 2003-0857, 2003.
[35]Godunov, S. K., "A difference scheme for numerical computation of discontinuous solution of hydrodynamic equations", J. Computational Physics, 32, 101-136, 1979.
[36]Hansen, R. P. and Forsythe, J. R., "Large and Detached Eddy Simulations of a Circular Cylinder using Unstructured Grids", AIAA Paper 2003-0775, 2003.
[37]Heidmann, J. D. and Hunter, S. D., "Coarse Grid Modeling of Turbine Film Cooling flows using Volumetric Source Terms", ASME Paper 2001-GT-0138, 2001.